Real Time Measurements of Single Bunch Phase and Length in the HERA Proton Storage Ring and the Observation of Multi-Bunch Oscillations

Elmar Vogel
Deutsches Elektronen-Synchrotron DESY, Hamburg, Germany

DESY Report No. DESY-HERA-00-08, 2000

Abstract

After the luminosity upgrade of the electron proton collider HERA, the proton bunch length will become relevant for the achievable luminosity. This is due to the enhancement of the effective cross section at the interaction region when the beta function and the bunch length have comparable magnitude, "hour-glass-effect" [1]. For a reduction of the bunch length, a better understanding of the longitudinal beam dynamics is essential. We developed a diagnostic system which permits real time measurements of bunch phase and length for all 180 bunches during one turn. One can also observe multi-bunch oscillations during acceleration which are correlated with an increase of the bunch length.

Moreover the system provides the signals needed for RF feed-forward and a multi-bunch feedback.

In this paper the technical setup is described and first measurements are shown.

1 INTRODUCTION

The HERA proton storage ring has 220 possible bunch positions 96 ns apart, 180 of which are occupied. The accelerator is shown in figure 1.

To inject 180 proton bunches into HERA, three PETRA fillings of 60 proton bunches must be transferred. The rise time of the injection kickers requires a gap of 5 bunch positions (480 ns) between the successive trains of 60 bunches. After the third 60 bunch train there is a gap of 15 bunch positions needed for the dump kicker at 920 GeV[1].

At the injection energy of 40 GeV the RF buckets are provided by a 52 MHz RF system. During ramping to 920 GeV a 208 MHz RF system takes over. The reasons for this double RF are the bucket matching during injection from PETRA [3, 4], and the longitudinal compression of the bunches by the steeper potential of the 208 MHz system at high energy.

Typical FWHM bunch lengths[2] after injection are 2.4 ns, during ramping the lengths are reduced to 1.6 ns by the compression of the 208 MHz RF System. Under the assumption of emittance conservation one would expect a bunch length of $l_{920\,\mathrm{GeV}} \approx 0.27\, l_{40\,\mathrm{GeV}}$ i.e. ≈ 0.6 ns. This means that there are processes during the ramp which increase the longitudinal emittance.

To understand this undesirable phenomenon it is necessary to study the longitudinal beam dynamics together with the technical properties of the storage ring in more detail.

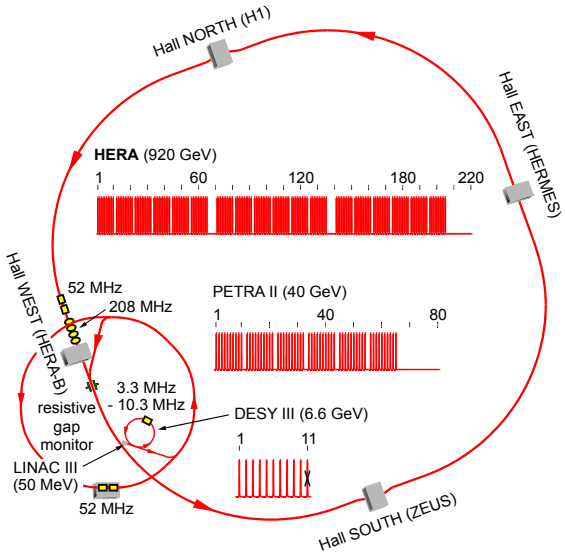

Figure 1: The proton accelerator complex at DESY with the various RF-Systems and the positions occupied by bunches. The gaps between the three bunch trains are needed for the build up of the fields in the injection and the dump kicker magnets.

2 EXISTING LONGITUDINAL BEAM DIAGNOSTICS

2.1 *Resistive Gap Monitor*

Two identical resistive gap monitors [5], installed in the HERA proton storage ring, are the basis of all longitudinal beam diagnostics. The monitors deliver time signals of the

[1] The rise time of the injection kickers is 200 ns. To build up the magnetic field of the dump kicker 800 ns are needed [2].

[2] Here we quote bunch length in the time domain. Since $\beta = \frac{v}{c} \geq 0.9997$ at HERA, the spatial lengths are given by multiplication with c.

bunches, with a time resolution of approximately 200 ps.

In figure 2 the working principle of a resistive gap monitor [6] is shown.

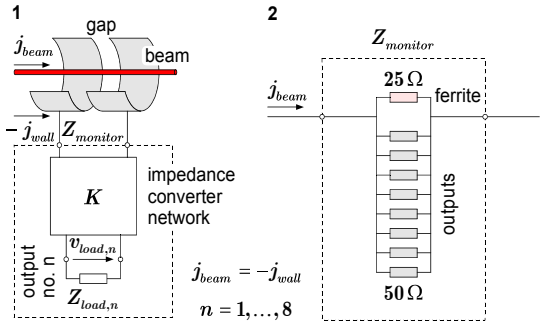

Figure 2: Working principle of a resistive gap monitor 1, and the equivalent network for calculation of the impedance as seen by the beam 2.

A beam with current j_{beam} induces in a smooth cylindrical vacuum chamber for $v = c$ the wall current $j_{wall} = -j_{beam}$. The vacuum chamber is separated by a small cylindrical gap, so that the wall current has to flow through an intermediate impedance converter network K. At the output no. n the network supplies the voltage signal $v_{load,\,n}$ to a load resistor $\mathrm{Re}\,(Z_{load,\,n})$. This signal is related by the monitor sensitivity factor S_n to the beam current j_{beam}:

$$v_{load,\,n} = S_n \; j_{beam} \tag{1}$$

When passing the monitor the beam loses the power $P_{monitor} = j_{beam}^2 \; \mathrm{Re}\,(Z_{monitor})$ and the network supplies the power $P_{load,\,n} = v_{load,\,n}^2 \,/\, \mathrm{Re}\,(Z_{load,\,n})$ at the output n. Hence the sensitivity is

$$S_n = \sqrt{\mathrm{Re}\,(Z_{load,\,n}) \; \mathrm{Re}\,(Z_{monitor}) \; \frac{P_{load,\,n}}{P_{monitor}}}. \tag{2}$$

In figure 3 the assembly of the monitor is shown. Eight 50 Ω outputs are arranged around the gap. A coaxial structure enclosing the vacuum chamber is loaded at the end with ferrites, to suppress reflections over a wide range of frequencies. The load of the ferrites amounts to 25 Ω. This

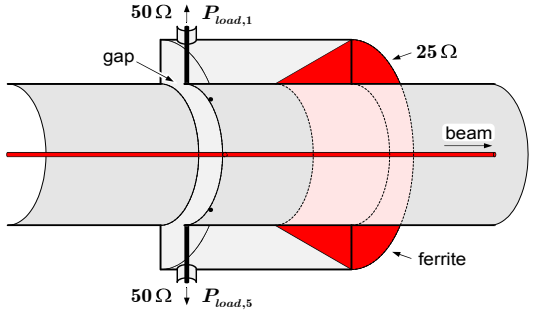

Figure 3: Resistive gap monitor

results in the equivalent network shown in figure 2, and the impedance, seen by the beam, is $Z_{monitor} = 5\,\Omega$. At one output the power of $P_{load} = \frac{1}{10} P_{monitor}$ is supplied, therefore the sensitivity factor is

$$S_n = \sqrt{50\,\Omega \; 5\,\Omega \; \frac{1}{10}} = 5\,\Omega. \tag{3}$$

The signals at the individual outputs depend on the horizontal and vertical beam position. This dependence can be eliminated by combining four outputs crosswise with resistive power combiners [7]. Resistive power combination results in a power loss of 50% in each combiner, i.e. the combination of four outputs yields the same power as a single output. Therefore the sensitivity is again 5 Ω.

2.2 *Narrow Band Phase Measurements*

Several narrow-band diagnostic methods to measure the beam phase are implemented in HERA. The principle is shown in figure 4.

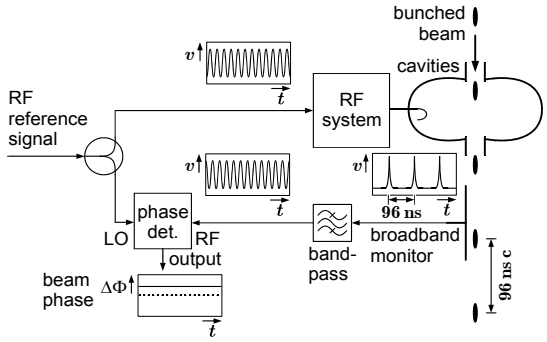

Figure 4: Principle of narrow-band beam phase measurements.

The bunched beam passes one of the resistive gap monitors and induces narrow output signals. These signals excite oscillations in a band pass filter whose central frequency is identical to the RF reference, hence the phase between these oscillations and the RF reference, measured with a phase detector, is equal to the beam phase. High accuracy in the phase measurement is obtained by averaging over many bunches, achieved either by a narrow band width of the band pass filter or by using low pass filters at the output. These systems are inadequate for the observation of multi-bunch oscillations, in particular the signal vanishes for out-of-phase synchrotron oscillations.

Two control loops are installed to damp synchrotron oscillations in HERA [8, 9, 10]. Both loops have phase detection units as described.

2.3 *Longitudinal Bunch Shape Measurements*

Sampling of the longitudinal bunch shape supplies information about single bunches [5].

The signal from a resistive gap monitor is transferred via a 35 m long 1 5/8" Flexwell cable to a Tektronix (TEK)

SCD5000 oscilloscope, with an analog bandwidth of 4.5 GHz and a digital resolution of 12.5 GHz. In figure 5 different bunch shapes, recorded with this device are presented.

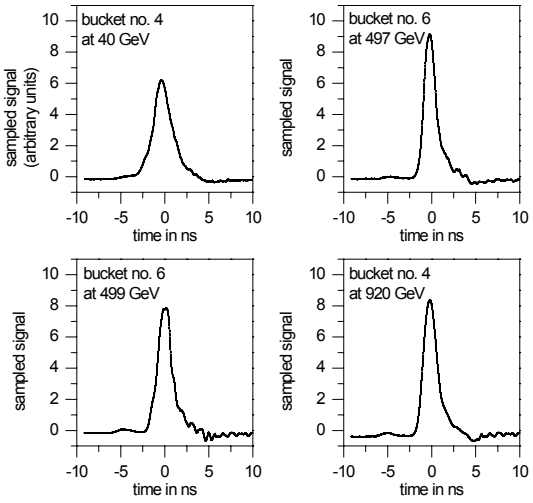

Figure 5: Different longitudinal bunch shapes, taken by sampling the signal of a broadband resistive gap monitor with a TEK SCD5000 oscilloscope.

The setup is very useful for the observation of selected bunches, but the SCD5000 has an effective dead time of about 500 ms. In practice one gets a bunch shape every second. This acquisition rate is too low to observe synchrotron oscillations with a typical frequency of 25 Hz.

The accuracy of the bunch phase measurement is directly connected to the jitter of the trigger signal provided to the oscilloscope. Since the jitter of the HERA timing is about ± 50 ps the maximum phase error is $\pm 3.6°$ with respect to a 208 MHz RF bucket. This is too inaccurate.

The dead time problem can be solved by using a fast frame oscilloscope, which is triggered on the same bunch every 100th revolution, see e.g. [3]. This technique is also often used for phase space tomography [11, 12, 13].

There is no easy way to implement the simultaneous observation of all bunches in HERA.

Considering all this, the setup of a new diagnostic tool to measure all bunch phases and length synchronous was indispensable.

3 REAL TIME MEASUREMENTS OF SINGLE BUNCH PHASE AND LENGTH

The resistive gap monitor is located behind the injection point near the Hall West where the proton beam is transferred from PETRA to HERA. A future feed-forward system for beam-loading compensation at injection would use this monitor.

limiter:	IN → OUT	$V_{OUT}(t) = \begin{cases} V_{lim} & \text{for } V_{IN}(t) > V_{lim} \\ -V_{lim} & \text{for } V_{IN}(t) < -V_{lim} \\ V_{IN}(t) & \text{else} \end{cases}$
90° phase shift:	IN → 90° OUT	$\mathbf{v}_{OUT}(t) = -i\,\mathbf{v}_{IN}(t)$
mixer:	RF, IF, LO	$\mathbf{v}_{IF}(t) = \frac{1}{2}\mathbf{v}_{LO}(t)\,\mathbf{v}^*_{RF}(t)$
two way 0° power splitter:	IN → 0° → OUT, OUT	$\mathbf{v}_{OUT}(t) = \frac{1}{\sqrt{2}}\mathbf{v}_{IN}(t)$
two way 90° power splitter:	IN → 90° → OUTI, OUTQ	$\mathbf{v}_{OUTI}(t) = \frac{1}{\sqrt{2}}\mathbf{v}_{IN}(t)$ $\mathbf{v}_{OUTQ}(t) = -\frac{i}{\sqrt{2}}\mathbf{v}_{IN}(t)$

Table 1: Mode of action of RF components used in phase detectors and I/Q demodulators.

3.1 Bunch Phase

The bunch phase is the RF phase deviation between the bunch center and the bucket minimum. We have to determine this phase for every bunch in a long train.

This is possible with a band-pass filter which has a decay time well below the 96 ns separation between two bunches. An I/Q demodulator is used to obtain the phase in the full range from $-180°$ to $180°$. The I/Q demodulator requires two analog-to-digital converters (ADCs), but the resulting data structure is an advantage for a digital control system, since successive data points correspond to the real and imaginary part of the angular pointer of the signal, and matrix multiplication can be used for the evaluations.

To understand the functioning and advantages of an I/Q demodulator, I first describe the principle of a phase detector.

In electrical engineering it is conventional to present a RF voltage $v_{RF}\,(t)$ by an angular pointer $\mathbf{v}_{RF}(t)$

$$\begin{aligned} v_{RF}(t) &= \mathrm{Im}\left[\mathbf{v}_{RF}(t)\right] \\ &= V_{RF}\,(t)\sin\left[\omega_{RF}\,t + \varphi_{RF}\,(t)\right], \end{aligned} \quad (4)$$

where $V_{RF}(t)$ is the amplitude and $\varphi_{RF}(t)$ the phase of the RF signal. Table 1 shows the action of the RF components, included in phase detectors and I/Q demodulators, in terms of angular pointers.

The RF components of a phase detector are a limiter, a low pass filter, a controllable phase shifter and a frequency mixer see figure 6. The output signal of the phase detector should depend only on the phase shift between the RF and the local oscillator LO input. For this reason the amplitude of the RF signal is first limited to a constant value. Higher harmonics generated by the limiter are damped by a low

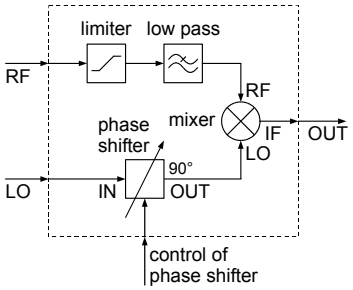

Figure 6: Principle of a phase detector.

pass filter. The resulting signal is mixed with the LO signal in a frequency mixer. Before doing this, the phase of the LO signal is shifted by a controllable phase shifter by 90°.

We get the output signal

$$v_{OUT}(t) = \frac{1}{2} V_{LO}\, V_{lim}\, \sin\left[(\omega_{LO} - \omega_{RF})\, t + \right. \\ \left. + (\varphi_{LO} - \varphi_{RF}(t))\right]. \quad (5)$$

The LO frequency is set equal to the RF frequency $\omega_{LO} = \omega_{RF}$ and for small phase deviations $|\varphi_{LO} - \varphi_{RF}(t)| \ll 1$ the sine function is linearized:

$$v_{OUT}(t) \approx \frac{1}{2} V_{LO}\, V_{lim}\, [\varphi_{LO} - \varphi_{RF}(t)] \quad (6)$$

Phase measurements with a phase detector suffer from several sources of errors. In practice the phase $\varphi_{LO} - \varphi_{RF}(t)$ consists of a constant and a time varying part, which one is interested in. First the constant part is subtracted by tuning the phase shifter. Large phase deviations lead to errors because of the replacement of the sine by its argument. A limiter also contains capacitive components which lead to a phase shift of the output signal, dependent on the input amplitude. Finally one has to measure $\frac{1}{2} V_{LO}\, V_{lim}$ for the calibration. Phase measurements with an I/Q demodulator avoid these problems.

An I/Q demodulator consists of two frequency mixers, a two way 0°power splitter, and a two way 90°power splitter, see figure 7.

The demodulator outputs are

$$v_Q(t) = \frac{1}{2\sqrt{2}} V_{LO}\, V_{RF}(t)\, \sin\left[(\omega_{LO} - \omega_{RF})t + \right. \\ \left. + (\varphi_{LO} - \varphi_{RF}(t))\right] \quad (7)$$

$$v_I(t) = \frac{1}{2\sqrt{2}} V_{LO}\, V_{RF}(t)\, \cos\left[(\omega_{LO} - \omega_{RF})t + \right. \\ \left. + (\varphi_{LO} - \varphi_{RF}(t))\right]. \quad (8)$$

In the special case $\omega_{LO} = \omega_{RF}$ one speaks of down-conversion to the base band. We get full information about the amplitude $V_{RF}(t)$ and phase $\varphi_{RF}(t)$ of the RF signal $v_{RF}(t)$ at the demodulator outputs.

The beam monitor signal of a single bunch excites an oscillation in a broadband 52 MHz band pass filter, which

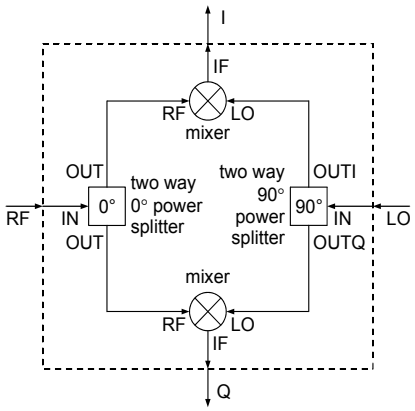

Figure 7: Principle of an I/Q demodulator.

is analyzed with an I/Q demodulator by down-conversion to the base band, using the RF frequency as local oscillator. Before sampling the I and Q signals with two ADC channels they are smoothed with low pass filters.

The correct sampling time is given by the condition that the expression $\sqrt{(v_I(t))^2 + (v_Q(t))^2}$ assumes its maximum. In this case we get the 52 MHz Fourier component of the bunch signal by

$$A_{52,\,meas} = \max\left[\sqrt{(v_I(t))^2 + (v_Q(t))^2}\right] \\ \equiv \sqrt{(v_{I,\max})^2 + (v_{Q,\max})^2} \quad (9)$$

$$A_{52} = C_{52}\, A_{52,\,meas} \quad (10)$$

and the phase[3] by

$$\Delta\phi = \arctan \frac{v_{Q,\max}}{v_{I,\max}} + \Delta\phi_{\mathit{offset}}. \quad (11)$$

where C_{52} is the overall gain in the circuit and $\Delta\phi_{\mathit{offset}}$ the phase offset between RF and LO inputs.

The following contradictory conditions must be fulfilled by the band pass filter:

1. The remaining RF oscillation in the filter must be small when the next pulse arrives. This means, the decay time of the RF signal in the filter has to be sufficiently small e.g. the bandwidth has to be large.

2. After the I/Q demodulator and the low pass filters a certain period of time is necessary for sampling at the signal maximum. For slowly varying signals the analog digital conversion is less sensitive to jitter in the ADC timing signals. For this reason larger decay times of the RF signal in the filter are desirable which imply a small bandwidth of the filter.

[3] In longitudinal beam dynamics the bunch phase is usually denoted by ϕ. We measure the phase $\Delta\phi = \phi - \phi_s$ with respect to the bucket minimum, which is equal to the phase of the synchronous particle ϕ_s.

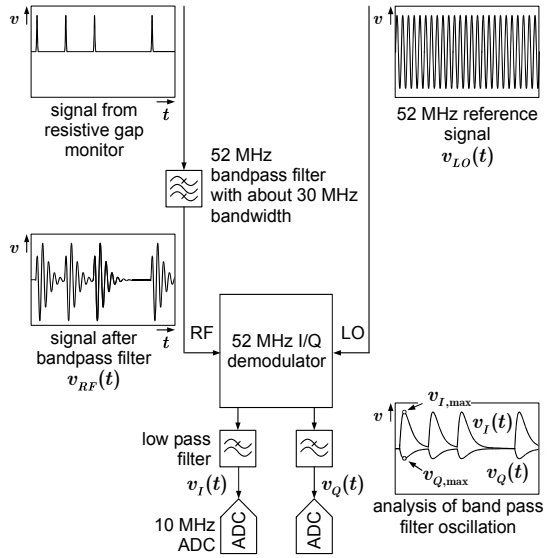

Figure 8: Measurement principle of the phase and amplitude of the 52 MHz Fourier component of a single bunch signal: The signal from the resistive gap monitor excites an oscillation in a band pass filter, which decays before the next bunch passes the monitor. The I/Q demodulator determines the in-phase (I) and out-of-phase (Q) components of the bunch induced oscillation, referred to the 52 MHz reference frequency.

center frequency:	52.041 MHz
design type:	series connection of two Butterworth filters of first order, importand is a constant cycle duration
bandwidth (6 dB):	25 MHz
input frequency:	DC to 4.2 GHz
pass band ripple:	$< \pm 0.2$ dB
impedance:	50 Ω at in- and output
insertion loss:	< 1 dB
dynamic range:	< -80 dBm to > 0 dBm
operating temperature:	-10 °C to 85 °C
connectors:	SMA

Table 2: Properties of 52 MHz band pass filter.

3. For useful phase information the filter should not ring and the cycle duration should be constant. To have no ringing effects in a filter, the progression of the phase over the frequency has to be a monotone and smooth function.

Simulations based on measured bunch shapes showed that two Butterworth filters of first order in series fulfill these criteria. The filter specification is given in table 2.

The filter was custom designed from a company according to these specifications.

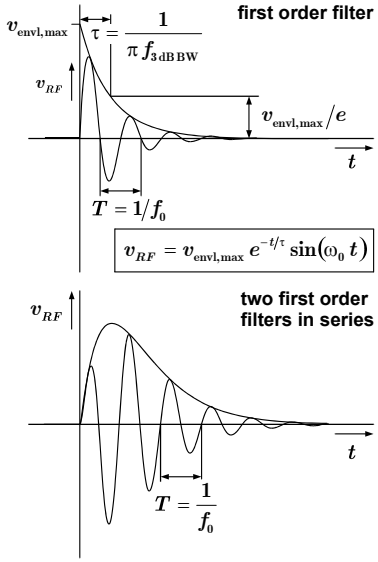

Figure 9: Response of an ideal 52 MHz band pass filter and a series connection of two band pass filters, each of first order, to an impulse excitation.

In figure 8, some technical details have been omitted: amplifiers for increasing signal levels and attenuators to suppress signal reflections.

An example of the bunch phase measurement is shown in figure 10. Here 10 bunches are measured without noticeable synchrotron oscillation and the measured phase values during a 0.52 s long period are plotted in a histogram, subtracting the individual time-averaged phase of each bunch. A Gaussian distribution is observed with a FWHM of 0.19°, with respect to the 52 MHz radio frequency. This number is an upper limit for the resolution of the detection system, since the phase noise of the bunched proton beam itself is included in the data.

3.2 Bunch Length

Two typical bunch shapes at 40 GeV and 499 GeV, as recorded with the fast oscilloscope, are shown in figures 11 and 12. An almost Gaussian shape is observed, even during strong synchrotron oscillations at 499 GeV. Under the assumption of a Gaussian bunch shape the experimental setup described here permits a bunch length determination in real time.

If we measure at least two Fourier coefficients at different frequencies we are able to calculate the bunch length:

Consider the monitor signal of a Gaussian bunch shape

$$A(t) = \frac{1}{\sqrt{2\,\pi}\sigma}\, e^{-\frac{1}{2}\frac{t^2}{\sigma^2}} \tag{12}$$

with the bunch length $l_{FWHM} = \beta\, c \sqrt{\ln 4}\, 2\, \sigma$. The Fourier

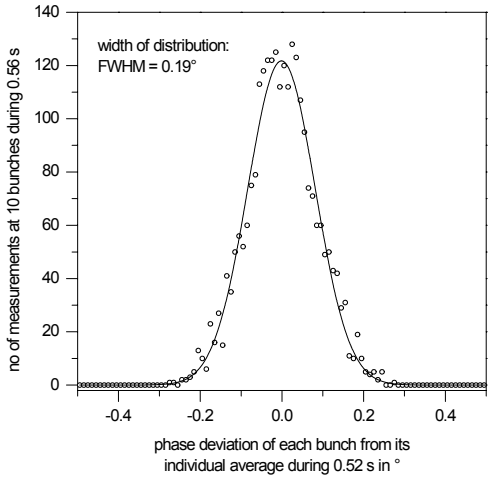

Figure 10: Relative measurement errors of single shot phase measurements.

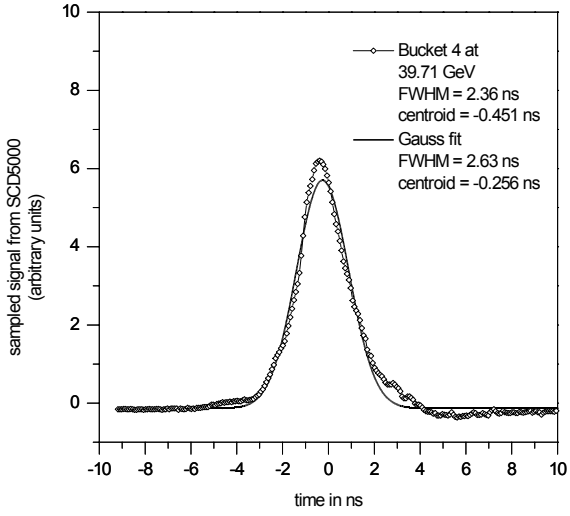

Figure 11: Bunch shape at 40 GeV.

component is

$$A(\omega) = \frac{\sigma}{\sqrt{2\,\pi}}\, e^{-\frac{1}{2}\sigma^2\omega^2}. \qquad (13)$$

Rearrangement of the ratio $\frac{A_1}{A_2} \equiv \frac{A(\omega_1)}{A(\omega_2)}$ yields the bunch length

$$l_{FWHM} = \beta\, c\, 2\,\sqrt{\ln 4}\sqrt{\frac{2}{\omega_2^2 - \omega_1^2}}\sqrt{\ln \frac{A_1}{A_2}}. \qquad (14)$$

In HERA the proton velocity is $v \approx c$, for simplification one can set $\beta = \frac{v}{c}$ to 1.

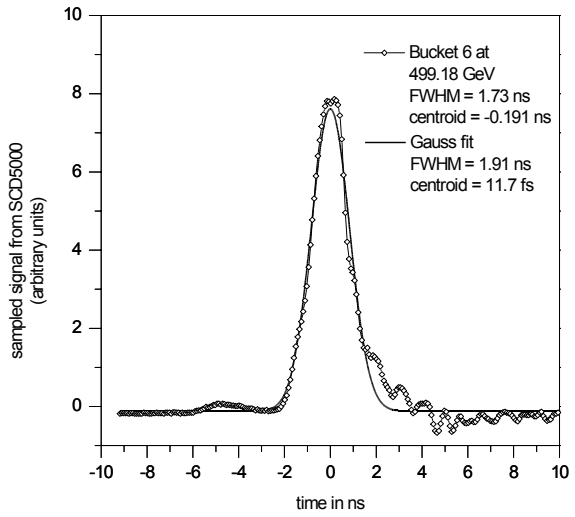

Figure 12: Bunch shape during bunch oscillations at 499 GeV.

From the phase measurement described in section 3.1, one obtains not only the bunch phase but also the amplitude of the 52 MHz Fourier coefficient of the longitudinal bunch signal. The natural choice for the second frequency is 208 MHz at HERA.

To measure the 208 MHz Fourier component a band pass filter is used whose specifications are identical to those given in table 2, except for the center frequency of 208 MHz. In figure 13 the bode diagrams of both band pass filters are shown.

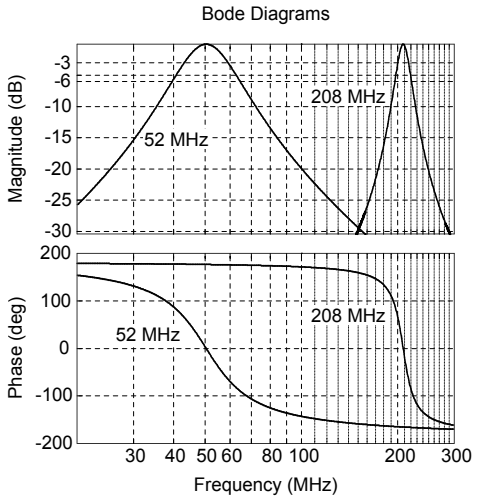

Figure 13: The Bode diagrams of the 52 MHz and 208 MHz band pass filters.

The output signal of the filter is detected by an RF diode, smoothed by a low pass filter, and then digitized by an

ADC. Figure 14 shows the setup.

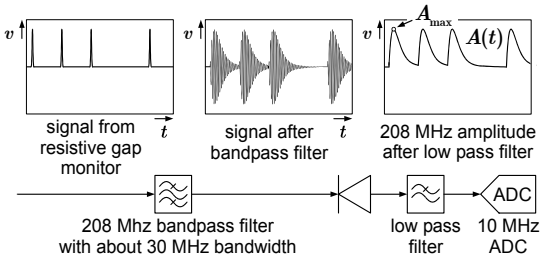

Figure 14: Principle of the 208 MHz bunch Fourier component measurement.

Taking into account the characteristic curve from the diode $F_{\mathrm{diode}}\left(A_{\max}\right) \propto A_{\max}^2$ and the different overall gains C_{52} and C_{208} at 52 MHz and 208 MHz, the bunch length is given by

$$l_{FWHM} = 2.63175\, ns \sqrt{\ln \frac{A_{52}}{A_{208}}} \qquad (15)$$

$$\frac{A_{52}}{A_{208}} = \frac{C_{52}}{C_{208}} \frac{A_{52,\,meas}}{A_{208,\,meas}}. \qquad (16)$$

In practice the ratio C_{52}/C_{208} is determined by comparing the results of this method with direct FWHM measurements using the TEK SCD5000 oscilloscope.

For long bunches the 208 MHz Fourier coefficient is small and the signal to noise ratio becomes unfavorable.

At a bunch length of 1.8 ns the measurement error of the single shot measurement is less than 5.2 ps, see figure 15.

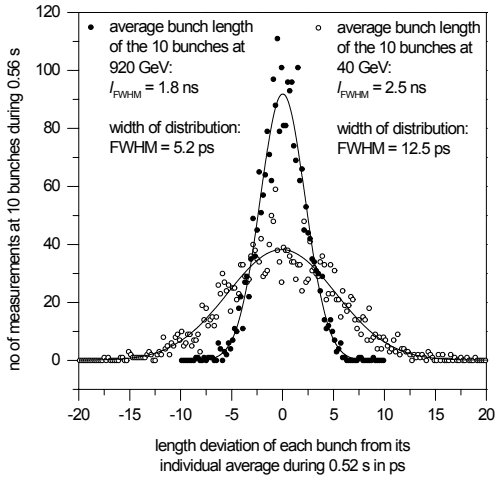

Figure 15: Length measurements of bunches with no observable oscillations.

Figure 16 shows the correlation of the average bunch length during a time interval of 0.56 s, measured with the method presented and the determination of the FWHM bunch length by analyzing the bunch shapes, recorded with the fast oscilloscope. A reasonable correlation is observed. The spread is mainly caused by multi-bunch oscillations during acceleration from 40 GeV to 920 GeV, where bunch length oscillations are always present. Therefore the results from the fast oscilloscope depend on the particular measurement times. The FWHM determination from the fast oscilloscope uses only the center peak and disregards the population in the head and tail of the bunch, while the real time method takes account of these particles. The disadvantage of the real time method is that particles spilled over into the neighboring 208 MHz RF buckets enhance the 208 MHz Fourier component and therefore the calculation of the bunch length (15) results in a shorter value.

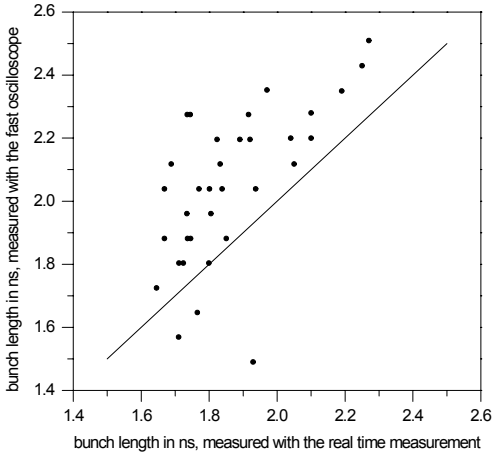

Figure 16: Correlation of the values determined by the real time bunch length measurement method and the FWHM measurement with the fast oscilloscope.

During the writing of this paper I found that the measurement of the bunch phase with two Fourier coefficients of the longitudinal bunch shape has also been attempted by [15].

4 MEASUREMENT OF MULTI-BUNCH OSCILLATIONS

4.1 Timing

For detection of multi-bunch oscillations the clock and trigger signals must be provided to the ADC boards in a special way.

The clock signals are rectangular signals with a frequency of 10.4 MHz, the bunch repetition frequency, deduced from the RF reference by counting RF waves with ECL gate arrays. The clock signals can be shifted under remote control in steps of 500 ps, to ensure that the ADCs sample the signal maxima.

Because of the low synchrotron frequency, 20 Hz to 60 Hz, it does not make sense to measure the bunch parameters every turn. In this case one synchrotron oscillation cycle would fill the ADC memory of 64 k (65536) samples per channel. The ADC boards used are able to start several times a measurement cycle with an eligible number of samples, 256 samples for each cycle are selected. Measuring every 104th revolution has turned out to be a good compromise between time and frequency resolution. A trigger signal is provided every 104th revolution, by dividing the beam revolution trigger (47.310 kHz) by 104. In this way, the phase and amplitude of an individual bunch are sampled with a frequency of 455 Hz, fast enough for the observation of bunch phase oscillations (20 Hz to 60 Hz) and length oscillations (40 Hz to 120 Hz). The total recording time is 0.56 s.

4.2 Data acquisition

Ground loops on the signal path which carry high frequency signals have been suppressed by using DC blocks. After down conversion of the signals DC blocks could not be used any more. Background noise could be removed by using sampled values from unoccupied bunch positions for an offset correction [16]. The dump gap consisting of 15 bunch positions was used for this purpose. Since the revolution frequency is 47.310 kHz, we suppress every unwanted signal modulation in the technical setup with a frequency lower than 47 kHz. Errors caused by net frequency and ground loops are suppressed rather well.

Several measurements were made with incomplete filling of the ring. To remove unoccupied bunch positions from the data, a minimum value of the 52 MHz Fourier component was required.

5 EXPERIMENTAL RESULTS

5.1 Multi Bunch Oscillations

On account of the beam loading transients, the bucket minima are not equidistant. This results in a shift of the bunch phasing with respect to the RF reference signal from one bunch to the next. Thus the first step for data presentation is the calculation of the average phase of each bunch during the measurement time of 0.56 s. The data are shown in figure 17. A systematic variation of the phase is seen along the three trains of 60 bunches.

During multi bunch oscillations a single bunch carries out phase oscillations with a typical amplitude of 2°about its average value. For a graphical representation only the phase deviations of each bunch from its average phase during the observation time are presented using a colored pixel plot . The two axes in figure 18 are the bucket position and time while the phase deviation from the average is indicated by the pixel color[4].

The presentation of bunch lengths is done in the same way, figure 19 and 20.

[4]Similar graphic representations have already been used at Fermilab.

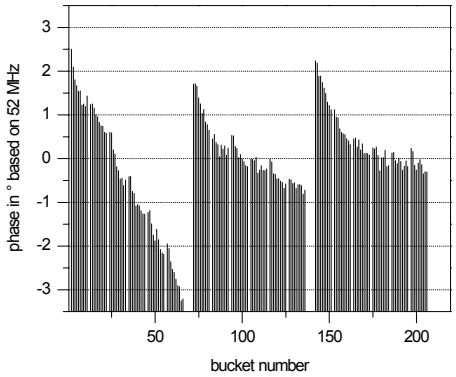

Figure 17: The average phase of each bunch during a measurement time of 0.56 s.

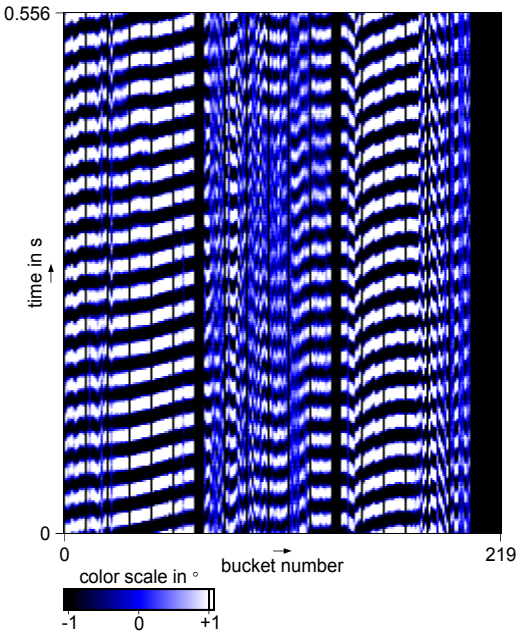

Figure 18: Multi bunch dipole oscillation at 499 GeV. The axes are the bucket position and time. The phase deviation from the average bunch phase with respect to 52 MHz is given by the pixel color.

With this diagnostic tool one observes multi bunch oscillations during every ramp of the proton storage ring. At energies above 300 GeV one sees the most impressive oscillations. Usual they persist up to 920 GeV. In the stored 920 GeV beam the multi bunch oscillations decay within half an hour. After the decay the pattern shown in figure 21 is obtained, which is characteristic of a quiet beam without measurable multi bunch oscillations remaining for the rest of the luminosity run.

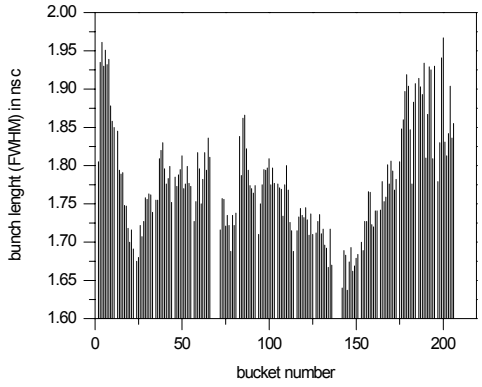

Figure 19: The average length of each bunch at 499 GeV during a measurement time of 0.56 s.

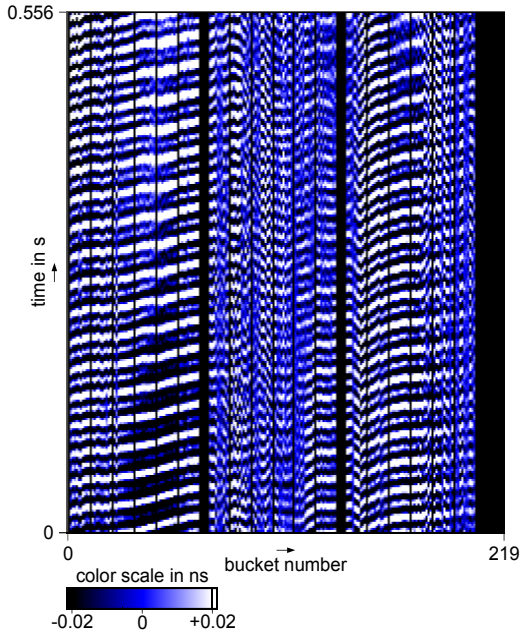

Figure 20: Multi bunch quadrupole oscillation at 499 GeV.

5.2 *Emittance Blow Up*

In figure 22 the average length of all bunches is plotted versus the time together with the energy. At the injection energy of 40 GeV one observes jumps related to the injection of the second and the third train from the pre-accelerator PETRA. On the ramp from 40 GeV to 920 GeV the optics is changed at various intermediate energies: 70 GeV, 150 GeV, 300 GeV and 675 GeV. The steps in the energy ramp are correlated with small jumps in the average bunch length and with multi bunch oscillations.

In a storage ring the longitudinal emittance is theoretically conserved. So the bunch lengthening is indicated better by calculating the longitudinal emittance. The longitudinal emittance is given by [14]

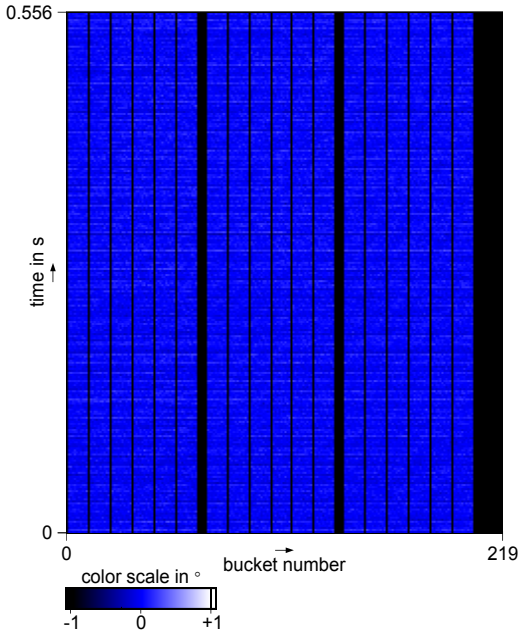

Figure 21: At stationary states of the storage ring one observe always a quiet beam. Here for example at 920 GeV.

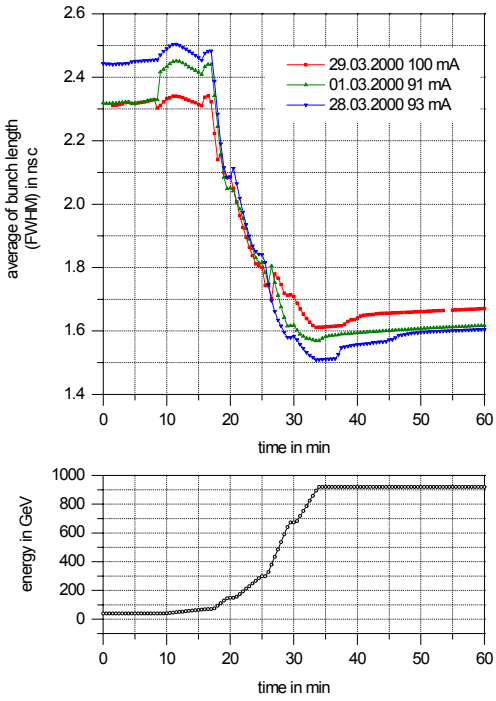

Figure 22: The change of the average bunch length during ramping form 40 GeV to 920 GeV, see text.

$$S_{FWHM} = \pi \, \Delta t_{FWHM} \, \Delta E_{FWHM} \tag{17}$$

with [17]

$$\Delta t_{FWHM} = \frac{1}{2} \frac{l_{FWHM}}{c} = \frac{\Delta \phi_{FWHM}}{\omega_{RF}} \tag{18}$$

$$\Delta E_{FWHM} = \beta \sqrt{\frac{2\,E_s}{\eta}} \sqrt{U\left(\Delta \phi_{FWHM}\right)} \tag{19}$$

ΔE_{FWHM} is the energy deviation, Δt_{FWHM} the time deviation of a particle with phase deviation $\Delta \phi_{FWHM}$, $\beta = \frac{v}{c}$, E_s the energy of the synchronous particle and $\eta = \frac{1}{\gamma_t^2} + \frac{1}{\gamma^2}$ the slip factor with $\gamma_t = 27.74$ and $\gamma = \frac{E_s}{E_0}$.

The voltage of the double harmonic RF System

$$V = V_{52} \sin \phi + V_{208} \sin 4\,\phi \tag{20}$$

creates a bucket potential

$$\begin{aligned} U\left(\Delta\phi\right) \quad = \quad & \frac{e}{2\pi} \frac{V_{52}}{h_{52}} \left(\sin \phi_s \left(\phi_s - \Delta\phi\right) + \right. \\ & + \cos \phi_s - \cos \Delta\phi) + \\ & + \frac{e}{2\pi} \frac{V_{208}}{4\,h_{52}} \left(\sin 4\,\phi_s \left(4\,\phi_s - \Delta\phi\right) + \right. \\ & \left. + \cos \phi_s - \cos \Delta\phi\right). \end{aligned} \tag{21}$$

ϕ_s is the synchronous phase and $\Delta\phi$ the phase deviation. To simplify the calculation of the longitudinal emittance using (17), (18), (19) and (21), the synchronous phase ϕ_s was set to zero. The time-evolution of the emittance is plotted in figure 23.

One observes a strong increase from 40 GeV to 920 GeV. To get more insight, the time derivative of the emittance is plotted in figure 24. It exhibits strong maxima at 123 GeV and 499 GeV. These are associated with multi bunch oscillations of large amplitude. A close look at figure 24 reveals that the stepwise increase in the emittances do not occur during the optics change at fixed energy but rather in the acceleration periods in between optic changes.

Obviously an optics change at constant energy does not cause multi-bunch oscillations. Possible reasons for the excitations of oscillations during acceleration are chromaticity effects, errors in the tracking between the field in the superconducting bending magnets and the radio frequency and the effects of passive impedances caused by steps in the beam pipe, or of active impedances like the RF feed-back systems. Investigations concerning possible multi-bunch instabilities in HERA are underway.

All pictures of multi bunch oscillations presented in this paper were taken at 29th March 2000 at 499 GeV where a big blow up of the longitudinal emittance took place.

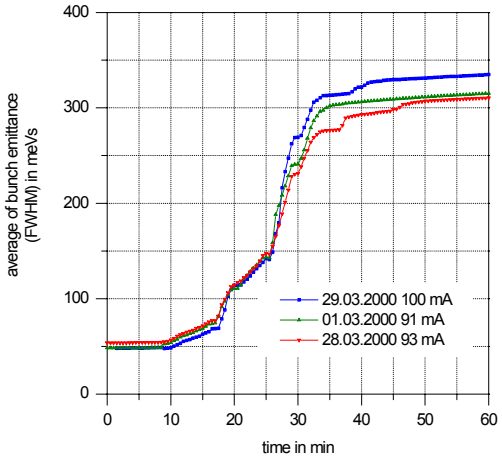

Figure 23: Evolution of the longitudinal emittance (FWHM) during the energy ramp from 40 GeV to 920 GeV.

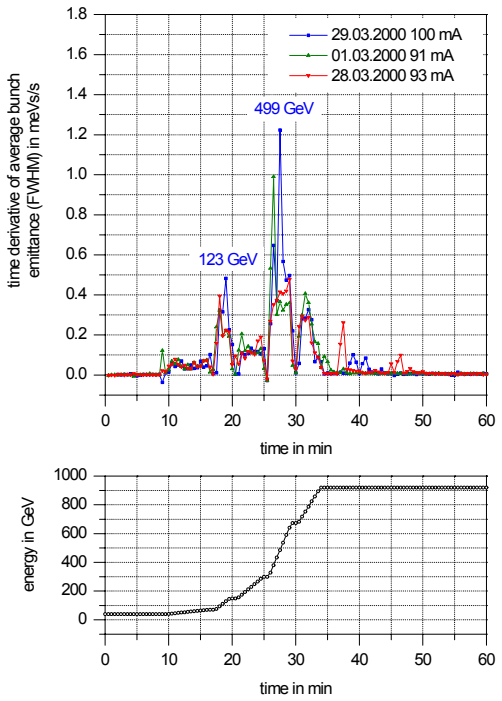

Figure 24: The time derivative of the longitudinal emittances is a measure of the emttiance blow up.

6 CONCLUSION

In this paper the technical setup to measure the proton bunch phase and the length of each individual bunch during one HERA revolution has been described. The most

important parts of this setup are custom designed filters for measuring the 52 MHz and 208 MHz Fourier components of the individual bunch shapes. A special timing of ADC boards permits the measurement of multi-bunch dipole and quadruple oscillations.

As a first result the simultaneous appearance of huge multi-bunch oscillations and emittance blow up was shown.

7 ACKNOWLEDGMENTS

Many people were involved in the on-going realization of the hard- and software. I would like to thank Peter Albrecht, Ralf Apel, Josef Baran, Wolfgang Bensch, Bernd Closius, Guenter Delfs, Hans-Thomas Duhme, Peter Gasiorek, Serguei Goloborodko, Torsten Grevsmuehl, Steve Herb, Gerd Hochweller, Andrej Kholodniy, Manfred Luehmann, Jorgen Lund-Nielsen, Tomasz Plawski, Willi Radloff, Rainer Saust, Victor Soloviev, Andreas Sommer, Klaus-Ulrich Tode, Richard Wagner, Manfred Wendt, Hong Gong Wu and Xiang Zeng.

For helpful discussions I would like to thank Alexander Gamp, Uwe Hurdelbrink, Wilhelm Kriens, Michiko Minty and Stefan Simrock. I would also like to thank Peter Schmueser for his advice during writing this paper.

I would like to thank as well the Deutsches Elektronen-Synchrotron DESY for providing all the necessary resources.

8 REFERENCES

[1] M. A. Furman, "The hourglass reduction factor fo asymmetric colliders", Asymmetric B-Factory collider Note No. SLAC-ABC-41-REV (1991)

[2] personal communication with J. Rümmler, DESY (1999)

[3] W. Kriens, "PETRA Bunch Rotation", in *Proceedings of the Particle Accelerator Conference, Vancouver, Canada,* 1997, (DESY Report No. DESY-M-97-10N, 1997)

[4] G. Wiesenfeldt, "Untersuchungen zur longitudinalen Strahlanpassung beim Protonentransfer von PETRA nach HERA", Diplomarbeit, University of Hamburg (1995)

[5] G. Lopez *et al*, "Observation of Proton Bunch Behavior in HERA", in Int. J. Mod. Phys. A, Proc. Suppl. 2A, p. 251 (1993), identical with *Proceedings of International Conference on High Energy Accelerators, Hamburg, Germany,* 1992

[6] D. Bussard, "Schottky Noise and Beam Transfer Function Diagnostics", in *Proceedings of CERN Accelerator School - Fifth Advanced Accelerator Physics Course, Rhodes, Greece,* 1993 (CERN Report No. CERN-95-06-vol.2, p. 758, 1995)

[7] Private communication with M. Wendt from DESY. His signal combination method is based on a idea already used at CERN. (2000)

[8] A. Gamp, "Servo Control of RF Cavities under Beam Loading", in *Proceedings of CERN Accelerator School - RF Engineering for Particle Accelerators, Oxford, United Kingdom,* 1991 (CERN Report No. CERN-92-03-vol.2, p. 396, 1992)

[9] W. Kriens, "Neue Kontrollen für die Frequenz- und Transfersteuerung bei HERA", in *DESY Accelerator Operation Seminar Grömitz, Germany,* 1999 (DESY Report No. DESY-HERA-99-04, p. 405, 1999)

[10] W. Kriens, "Neue Kontrollen für die Frequenzsteuerung und Synchronisation bei HERAp" in *DESY Accelerator Operation Seminar Grömitz, Germany,* 2000 (DESY Report No. DESY-M-00-05, 2000)

[11] http://t.home.cern.ch/t/tomograp/www/

[12] S. Hancock, P. Knaus, M. Lindroos, "Thomographic Measurements of Longitudinal Phase Space Density", in *Proceedings of the European Particle Accelerator Conference, Stockholm, Sweden,* 1998

[13] S. Hancock, S. Koscielniak, M. Lindroos, "Longitudinal Phase Space Tomography with Space Charge", CERN Report No. CERN-PS-2000-021-RF (2000)

[14] D. A. Edwards, M. J. Syphers, An Introduction to the Physics of High Energy Accelerators (John Wiley & Sons, 1993)

[15] C. Boccard, T. Bogey, J. P. Papis and L. Vos, "Intensity and Bunch Length Measurement for Lepton Beam in the Injection Lines of the SPS and LEP", in *Proceedings of Second European Workshop on Beam Diagnostics and Instrumentation for Particle Accelerators (DIPAC'95), Lübeck-Travemünde, Germany, 1995,* (CERN Report No. CERN SL/95-58 (AP), 1995)

[16] Y. Chernousko suggested this idea, DESY (1999)

[17] W. Pirkl, "Longitudinal Beam Dynamics", in *Proceedings of CERN Accelerator School - Fifth Advanced Accelerator Physics Course, Rhodes, Greece,* 1993 (CERN Report No. CERN-95-06-vol.1, p. 233, 1995)

[18] W. Kriens, M. Minty, "Longitudinal Schottky Monitoring for Protons in HERA", in *Proceedings of the European Particle Accelerator Conference, Vienna, Austria,* 2000